# ROCK PHYSICS MODELING WITH MINERALOGICAL INVERSION IN SANDSTONE RESERVOIR

Fábio Júnior Damasceno Fernandes [1], Leonardo Teixeira [1,2],
Antonio Fernando Menezes Freire [1,3], and Wagner Moreira Lupinacci [1,3]

[1]Universidade Federal Fluminense - UFF, Geology and Geophysics Department,
Exploratory Interpretation and Reservoir Characterization Group (GIECAR), Niterói, RJ, Brazil
[2]Petrobras, Rio de Janeiro, RJ, Brazil
[3]National Institute of Science and Technology of Petroleum Geophysics, Niterói, RJ, Brazil

*Corresponding author email: fabiojdf@id.uff.br

ABSTRACT. Reservoir characterization is a valuable tool for the oil and gas industry. A better understanding of the reservoir demands the integration of petrophysical properties and elastic parameters. This integration is commonly performed with the aid of rock physics models. The elastic properties of solid phase components are important parameters for rock physics model calibration. In this paper, we use an adaptation of mineralogical inversion to estimate the volumes of quartz, feldspar, and clay minerals that incorporate previously calculated clay volume and porosity. Clay volume estimation is performed from neutron and bulk density logs. We chose this method due to the presence of feldspar minerals in the reservoirs. Our workflow consists of petrophysics property estimation, mineralogical inversion, rock physics model calibration in Well A, and compressional wave velocity estimation in Well B. The mineralogical inversion in Well A provided average volumes of 64% quartz and 16% feldspar and previously estimated 20% clay minerals. When applied to Well B, the calibrated soft sand model is a better approximation for high porosity data points than the constant cement model, and the error between original and estimated logs is about 2.9%, suggesting that the approach can be extended to other wells in the study area.

Keywords: reservoir characterization; mineralogical inversion; rock physics models; compressional wave velocity estimation.

INTRODUCTION

Understanding the reservoir properties is fundamental in the hydrocarbon exploration and production phases. The well logs assist the assessment of clay volume, porosity, permeability, water saturation, and net pay for the characterization of siliciclastic reservoirs. Another important set of information for reservoir characterization is the elastic parameters of rock constituents. Rock physics models serve as a link between petrophysical properties and elastic parameters and can provide more assertive information on the behavior of reservoirs.

Rock physics models can be separated into empirical and theoretical. Empirical rock physics models search for empirical relations between dependent variables in each dataset. In the literature, several empirical models have been presented for specific datasets such as Pickett (1963); Raymer et al. (1980); Castagna et al. (1985); Han et al. (1986); Williams (1990). Greenberg and Castagna (1992) synthesized for various lithologies empirical transformations for multimineralic brine-saturated rocks composed of sandstone, limestone, dolomite, and shale.

Theoretical rock physics models are developed based on physical principles to explain in a simplified way the elastic behavior of rocks. Dvorkin and Nur (1996) used the contact theory between grains from Hertz (1882) and Mindlin (1949) and rock physics bounds of Hashin-Shtrikman (1963) to propose granular effective media models. Allo (2019) proposed an extension of these models including new modeling parameters such as matrix stiffness index, cement cohesion coefficient, contact-cement fraction, and laminated clay fraction.

Elastic properties of solid and fluid phases are fundamental inputs to theoretical models. Solid phase properties depend on the constituent minerals and their respective volumes (Avseth et al., 2005). In complex lithologies and in the presence of two or more minerals, it is essential to understand and estimate the variations over the investigation interval in the proportion of each mineral. By performing this evaluation, it is possible to obtain the effective elastic modulus using rock physics bounds. Savre (1963); Tixier and Alger (1967); Schmoker and Schenk (1988); and Amosu and Sun (2018) used well log analysis routines to solve an inverse problem to estimate mineral volumes over an interval. Doveton (1994) made a synthesis of the solutions of linear inverse problems for underdetermined, determined and overdetermined systems for mineral volume estimation.

This work proposes a workflow for rock physics model calibration and a model-based assessment of compressional wave log. This estimation required the knowledge of clay volume, porosity, and water saturation. To estimate clay volume, we propose an approach based on neutron and bulk density logs, as these logs are not sensitive to the radioactivity of the feldspar mineral present in arcosean sandstone. Then, an adaptation of the mineralogical inversion method for mineral volume estimation is carried out. We then perform the calibration of soft sand and constant cement models for compressional wave velocity in Well A, and apply them in Well B.

METHODOLOGY

The data used in this work were collected from two wells (A and B) located in Novo Campo de Jubarte, Parque das Baleias, Campos Basin (Figure 1). The investigation interval is the Eocene, comprising sandstones, shales, and marls (Winter et al., 2007). The workflow shown in Figure 2 was applied to both wells until the fluid substitution step. The calibration of the

rock physics models was performed in Well A. From the calibrated models, we performed the compressional wave velocity log modeling in Well B to validate the methodology. The steps of the proposed methodology are described in the next sections.

Petrophysics Property Estimation

Clay volume estimation is widely performed with the gamma-ray log (GR), which is linked to the natural radioactivity emitted from the rocks (Ellis & Singer, 2007). As shale has high clay mineral content, its natural radioactivity level tends to be high due to the presence of radioactive elements like potassium (K40). Therefore, the GR log has been very useful over time for distinguishing between sandstone and shale (Rider & Kennedy, 2002). However, in more recent rocks, the effects of diagenesis are smaller and they may have a higher presence of potassium-bearing minerals like feldspars and micas, providing high radioactivity unrelated to clay minerals (Bhuyan & Passey, 1994).

Bhuyan and Passey (1994) used bulk density and neutron logs to estimate clay volume. The clay volume estimation from these logs tends to be advantageous in formations without the presence of gas and with feldspar minerals, which is the case of the study area. This occurs because the neutron log is sensitive to the hydrogen present in clay minerals, while the bulk density log is not. Furthermore, quartz, feldspar, calcite and dolomite minerals do not have high hydrogen content. Paiva et al. (2019) and Fernandes et al. (2021) compared the clay volume estimation in siliciclastic intervals in the Campos Basin using the GR method with the neutron and bulk density one. The results showed that the method using neutron and density logs is more consistent with interpreted lithologies in feldspar-rich reservoirs.

In this work it is presented an approach for clay volume estimation based on the neutron and bulk density logs. The equation used is given by:

$$\frac{VCLND}{X3 - X4} = \frac{X_1 - X_2}{X_3 - X_4},\qquad(1)$$

with:

$$X_1 = (RHOB_{cl2} - RHOB_{cl1}) \times (NPHI - NPHI_{cl1}),$$

$$X_2 = (RHOB - RHOB_{cl1}) \times (NPHI_{cl2} - NPHI_{cl1}),$$

$$X_3 = (RHOB_{cl2} - RHOB_{cl1}) \times (NPHI_{clay} - NPHI_{cl1}),$$

$$X_4 = (RHOB_{clay} - RHOB_{cl1}) \times (NPHI_{cl2} - NPHI_{cl1}),$$

where $RHOB$ and $NPHI$ are the measurements of the neutron and bulk density logs, respectively, and the
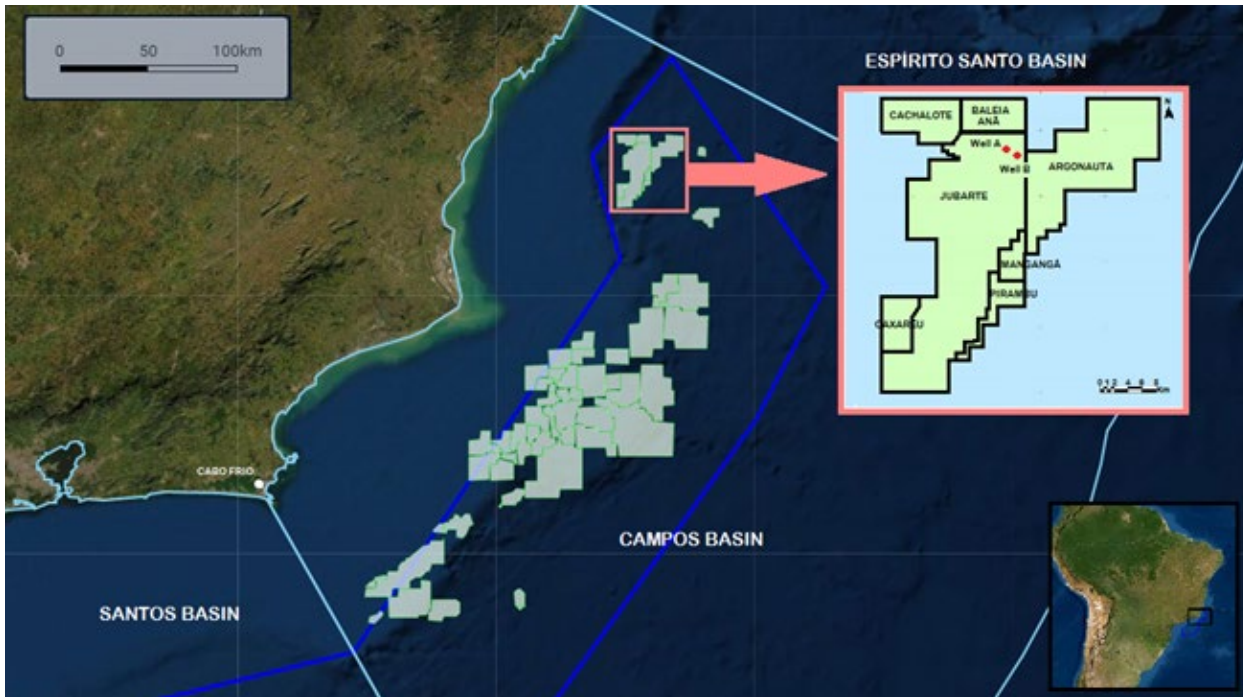
Figure 1: Location of Novo Campo de Jubarte within Campos Basin. Wells A and B in the study area are represented by circles.
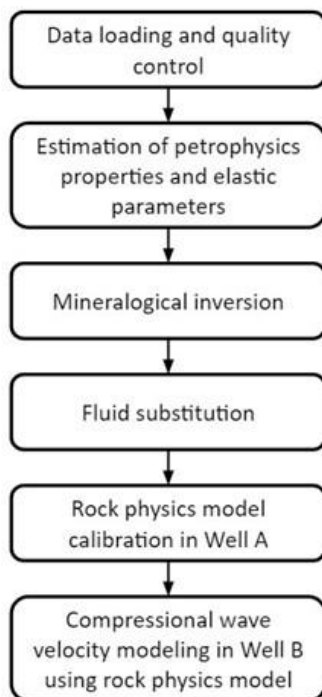

Figure 2: Proposed methodology and validation for modeling compressional wave velocity.

subscribed points $cl1$, $cl2$ and $clay$ are defined from the crossplot between the neutron and bulk density logs ([Figure 3](#)); the DRDN parameter is given by the following equation ([Guimarães et al., 2008](#); [Freire et al., 2020](#)):

$$DRDN = \left(\frac{RHOB - 2}{0.05}\right) - \left(\frac{0.45 - NPHI}{0.03}\right). \qquad (2)$$

The $DRDN$ log is performed as a discriminant between sandstone ($DRDN < 0$) and shale ($DRDN \geq 0$) ([Guimarães et al. 2008](#)). The points $cl1$ and $cl2$ correspond to clean sandstones and are defined from thresholds of the photoelectric factor, acoustic impedance and DRDN logs. From these values, a line (clean volume equals to 0%) is fitted using least squares regression. Point $cl1$ is defined on the intersection of this line with the quartz density line (2.65 g/cm³). Point $cl2$ represents the maximum values of the neutron and bulk density over the line of the clay volume equals 0%. Then, the clay point that represents 100% of the clay volume is defined. Finally, the clay volume lines 20%, 40%, 60%, 80% are drawn proportionally to the points $cl1$, $cl2$ and $clay$.

Neutron and bulk density logs are also used for calculation of the total ($PHIT$) and effective porosities ($PHIE$) (for more details, see, e.g., [Schön, 2015](#)). Porosity is an important petrophysical property that is usually related to elastic parameters in rock physics models. Another important reservoir property is water saturation. Its estimate was made from [Archie's equation (1942)](#):

$$S_w = \sqrt[n]{\frac{a \times R_w}{\varphi^m \times R_t}}, \qquad (3)$$

where the parameters tortuosity factor (a); cementation exponent (m); and saturation exponent (n) were defined as $a = 1$; $m = 2$; $n = 2$. These values are commonly used in sandstone reservoirs ([Hartmann and Beaumont, 1999](#)).
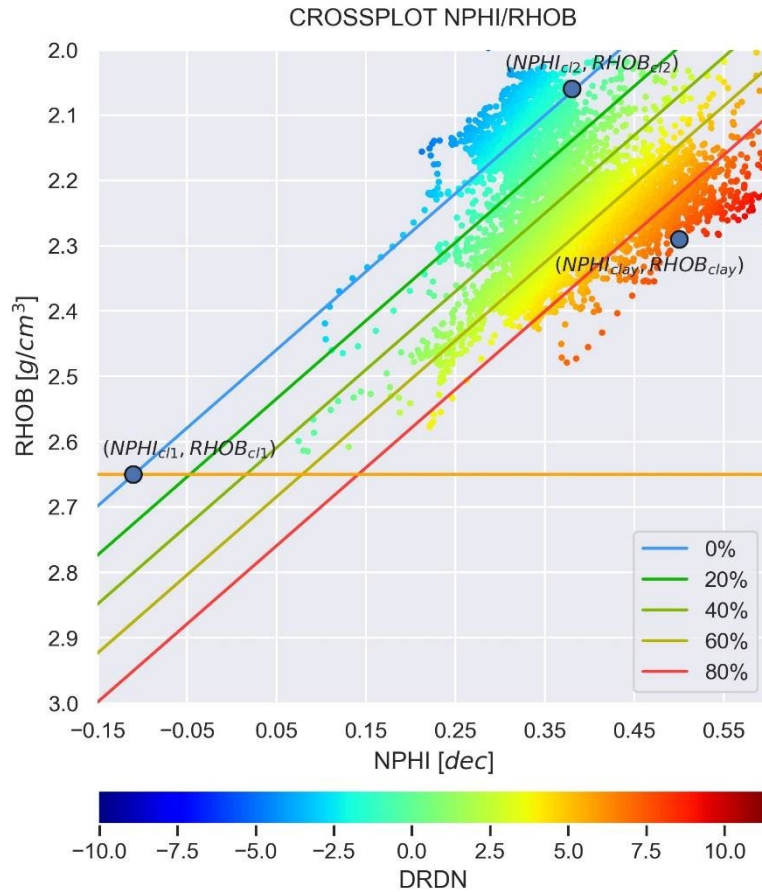
Figure 3: Graphical illustration of the procedure to estimate clay volume using neutron (NPHI) and bulk density (RHOB) logs. The crossplot is color coded by the DRDN log and it is showing a trend that follows the clay volume variations. These variations are graphically represented by the five lines shown. Higher values of DRDN were estimated close to the *clay* point $(NPHI_{clay}, RHOB_{clay})$ and lower values of DRDN were found close to the *cl2* point $(NPHI_{cl2}, RHOB_{cl2})$.

The formation water resistivity was obtained from laboratory data ($R_w = 0.0206$ ohm.m). As the fluid type plays an important role over the elastic parameters of rocks, a more accurate estimate of water and oil saturations is required in the approach of this work.

Mineralogical Inversion

The knowledge of rock-constituent mineral volumes is an important information for reservoir characterization because mineral volumes are used in fluid substitution and rock physics model calibration. The rigidity of minerals in the composition of the rock significantly influences the sensitivity of elastic parameters to fluid substitution.

[Doveton (1994)](#) synthesizes some methodologies already applied to estimate mineral volumes using well logs. Matrix operations applied to the logs transform data coordinates located in log space to composition space according to the equation:

$$CV = L, \tag{6}$$

where C is the matrix of the mineral properties related to the logs; V is the mineral volume vector to be estimated; and L is the vector of the well logs. This equation linearizes the model that relates rock properties with log measurements. To estimate the mineral volumes, it is necessary to perform the inverse process, given by the equation:

$$V = C^{-1}L, \tag{7}$$

where C^{-1} is the inverse of matrix C.

In cases where the number of logs is equal to the number of minerals (e.g., parameters) to be estimated present in the rock, the problem is characterized as a determined system. In our study, the number of logs is greater than the number of minerals to be estimated. Therefore, this is a case of an overdetermined linear problem. Considering that the residual is normally

distributed, and the errors are independent, the solution is given by the equation (Aster et al., 2013):

$$V = (C^T C)^{-1} C^T L. \tag{8}$$

As the mineralogical inversion works with log data in different units, it is necessary the introduction of a weight (regularization) function. Without this step, the estimated error on minimization tends to honor the logs that have a higher range of values (Doveton, 1994). With the addition of the diagonal weight matrix (W), the solution to the problem becomes:

$$V = (C^T W C)^{-1} C^T W L. \tag{9}$$

The matrix W can be estimated based on physical principles or using the standard deviation of data (Harvey et al., 1990).

Well logs are commonly used to estimate mineral volumes within an interval of interest. Savre (1963) applied a mineralogical inversion to West Texas Permian carbonate rocks. The logs chosen were neutron porosity, sonic, and bulk density to estimate volumes of dolomite, gypsum, anhydrite, and fluids. Tixier and Alger (1967) performed the estimation of anhydrite, calcite, and sulfur minerals and porosity in a sulfur extraction area in the Louisiana salt dome from bulk density, neutron, and sonic logs. Schmoker and Schenk (1988) also used the same logs to estimate volumes of quartz, dolomite, anhydrite, and porosity in an interval of dolomite and sandstone beddings of the Permian upper part of the Minnelusa Formation in Powder River basin, Wyoming.

The works mentioned above that used mineralogical inversion consider both the solid, which corresponds to minerals, and the fluid phases during the inversion process. This is a relevant consideration for this application given the difficulty in obtaining information about the clay minerals. Thus, the result of the inversion is volumes of all minerals and fluids that compose the rock. This work proposes an adaptation of the mineralogical inversion to incorporate previous estimations of clay volume and porosity. Therefore, during the inversion process, we sought to condition that the remaining mineral volumes is equal to:

$$V_{qtz} + V_{fld} = 1 - PHIE - VCLND, \tag{10}$$

where V_{qtz} and V_{fld} represent the volumes of quartz and feldspar, respectively.

According to Silva et al. (2008), arcosean sandstones associated with turbidite flows, in general, are basically composed of quartz, feldspar and clay. Due to the fact that clay volume and porosity are estimated from other methods, our approach performs the inversion only to quartz and feldspar volumes. To estimate these two minerals, we used the photoelectric factor, bulk density, compressional wave slowness and gamma ray logs. The direct modeling of the system to be inverted is:

$$[DT_i \ PE_i \ RHOB_i \ GR_i \ \gamma_i \ ] =$$
$$[DT_{qtz} \ DT_{fld} \ PE_{qtz} \ PE_{fld} \ RHOB_{qtz} \ RHOB_{fld} \ GR_{qtz} \ GR_{fld} \ 1 \ 1] \tag{11}$$
$$[V_{qtz,i} \ V_{fld,i}]$$

where γ_i corresponds to the values of $1 - PHIE_i - VCLND_i$.

It is important to emphasize why we use effective porosity and not total porosity in this approach. According to Ellis and Singer (2007), the estimated clay volume corresponds to the dry clay volume added to clay bound water (CBW). Clay bound water is removed from the effective porosity because it is assumed that CBW is not mobile during production. Despite the small quantitative difference, from a theoretical point of view, the correct porosity to be used in our approach is the effective one. The well logs and mineral properties used in mineralogical inversion are shown in Table 1. These parameters correspond to the measurements of each tool for the respective mineral.

Table 1: Table with constants adopted for quartz and feldspar in mineralogical inversion. Sources: http://www.webmineral.com and Mavko et al. (2009).

	Quartz	Feldspar
PE [b/e]	1.80	2.85
RHOB [g/cm³]	2.65	2.53
DT [us/ft]	55.5	69
GR [GAPI]	0	200.97

We performed the mineralogical inversion using the standard methodology for comparison. The standard methodology estimates the volumes of minerals (quartz, feldspar and clay minerals) and the volume of fluids. This approach was accomplished by

several authors (Savre, 1963; Tixier and Alger, 1967; Schmoker and Schenk, 1988; Doveton, 1994). The properties of the illite mineral were used for clay mineral inversion (http://www.webmineral.com and Mavko et al., 2009). The constants of pore-filling fluid were taken from Mavko et al. (2009). This case is also an overdetermined linear system that involves the application of equation 9 as part of the solution.

Fluid Substitution

Fluid substitution consists of understanding and predicting how the elastic properties of the rock change with the substitution of pore-saturating fluid. We delve into some theoretical details on fluid substitution in this section for the explanation of our approach. Rock physics bounds are one of those concepts. They represent the limit elastic property response engendered by a mixture of volume fraction of rock constituents. The most used are Voigt, Reuss, Voigt-Reuss-Hill and Hashin-Shtrikman bounds (for more details, see Avseth et al., 2005; Mavko et al., 2009; Dvorkin et al., 2014).

We calculated the Reuss bound to estimate the effective bulk modulus of the fluid phase, which is a harmonic mean weighted by the amount of each fluid (Avseth et al., 2005). The fluid in the reservoir is a mixture of oil and water. To obtain the properties of the oil, we used the equations of Batzle and Wang (1992). For the solid phase, we compared different limits and adopted the Hashin-Shtrikman bound to present the best fit with respect to the data. Gassmann (1951) introduced theoretical fluid substitution equations using rock bulk moduli. To the estimation of bulk modulus of fluid-saturared rock 2 ($K_{sat}^{(2)}$) as a function of bulk modulus of fluid-saturated rock 1 ($K_{sat}^{(1)}$), the bulk modulus of solid phase (K_s), the bulk modulus of fluid 1 ($K_f^{(1)}$), and the fluid 2 ($K_f^{(2)}$) and effective porosity (φ), the following equation is adopted (Avseth et al., 2005):

$$\frac{K_{sat}^{(2)}}{K_s - K_{sat}^{(2)}} - \frac{K_f^{(2)}}{\varphi\left(K_s - K_f^{(2)}\right)} = \frac{K_{sat}^{(1)}}{K_s - K_{sat}^{(1)}} - \frac{K_f^{(1)}}{\varphi\left(K_s - K_f^{(1)}\right)}. \qquad (12)$$

We consider that the shear modulus does not change in fluid substitution because it is a low viscosity fluid (Dvorkin et al., 2014). An adaptation of Gassmann's equation was presented by Mavko et al. (1995) to be used when there is no shear-wave sonic log. This equation is the same as equation 12, only

with the substitution of the bulk modulus parameters by the compressional modulus parameters. The compressional modulus (M) is given by:

$$M = Vp^2 . RHOB, \qquad (13)$$

where Vp is the compressional wave velocity. We use $M_{sat}^{(1)}$ for fluid substitution in Well B as it does not have the sonic shear log.

Rock Physics Model Calibration

Rock physics models are useful for estimating scenarios absent in wells to analyze the influence of facies, fluids, and porosity on the seismic amplitude (Avseth et al., 2005). We use the granular effective medium models (GEM), also called contact models (Dvorkin & Nur, 1996). These theoretical models consider the rock as a set of spherical grains, where the elastic properties are determined from the deformability and rigidity of the contact between grains. Most of these models are based on Hertz (1882) and Mindlin (1949) solutions for the elastic behavior of two spherical grains in contact. Contact models are mainly used in siliciclastics rocks, as it is a good approximation for the behavior of this type of rock.

Rock physics models always have limitations, and, in this case, the problem lies in the idealized form of the grains, which are spherical and of a specific size. Allo (2019) extends the theory of GEM models to better approximations, which requires more information from the rock that is only available from laboratory data. Some of modeling parameters that Allo (2019) introduces in his models are matrix stiffness index, cement cohesion coefficient, contact-cement fraction and laminated clay fraction.

We perform the constant cement and soft sand models calibration. Constant cement model (CCM) considers a reduction in the initial porosity due to the effect of cementation and, after certain porosity, the decrease of porosity is associated with the introduction of non-cementing particles in the porous space. The equations of CCM are (Dvorkin et al. 2014):

$$K_{const} = \left[\frac{\frac{\varphi}{\varphi_c}}{K_{cem} + \frac{4}{3}G_{cem}} + \frac{1 - \frac{\varphi}{\varphi_c}}{K + \frac{4}{3}G_{cem}}\right]^{-1} - \frac{4}{3}G_{cem}, \qquad (14)$$

$$G_{const} = \left[\frac{\frac{\varphi}{\varphi_c}}{K_{cem} + Z_{cem}} + \frac{1 - \frac{\varphi}{\varphi_c}}{K + Z_{cem}}\right]^{-1} - Z_{cem}, \qquad (15)$$

with

$$Z_{cem} = \frac{G_{cem}}{6}\left(\frac{9K_{cem} + 8G_{cem}}{K_{cem} + 2G_{cem}}\right), \qquad (16)$$

where the parameters K_{cem}, G_{cem} and Z_{cem} are obtained from the contact-cement model ([Dvorkin & Nur 1996](#)). For the soft sand model (SSM), K_{cem} and G_{cem} are replaced by the points in the Hertz-Mindlin model ([Mindlin, 1949](#)), that is:

$$K_{HM} = [\frac{n^2(1-\varphi_c)^2 G^2}{18\pi^2(1-v)^2}P]^{\frac{1}{3}}, \qquad (17)$$

$$G_{HM} = \frac{5-4v}{5(2-v)}[\frac{3n^2(1-\varphi_c)^2 G^2}{2\pi^2(1-v)^2}P]^{\frac{1}{3}}. \qquad (18)$$

The equations for the CCM and SSM are similar. However, in the CCM, the point in the Hertz-Mindlin model is not used to link the critical porosity to the mineral point. Instead, the elastic modulus is used at the point where the loss of porosity is no longer dominated by the cement effect. We calibrated the granular effective model for dry rock. Thus, it is necessary to carry out fluid substitution on the model results to simulate the in-situ saturation using Gassmann's equations ([equation 12](#)). An example of the behavior of the elastic parameter of CCM for dry rock and different cement levels is illustrated in [Figure 4](#).
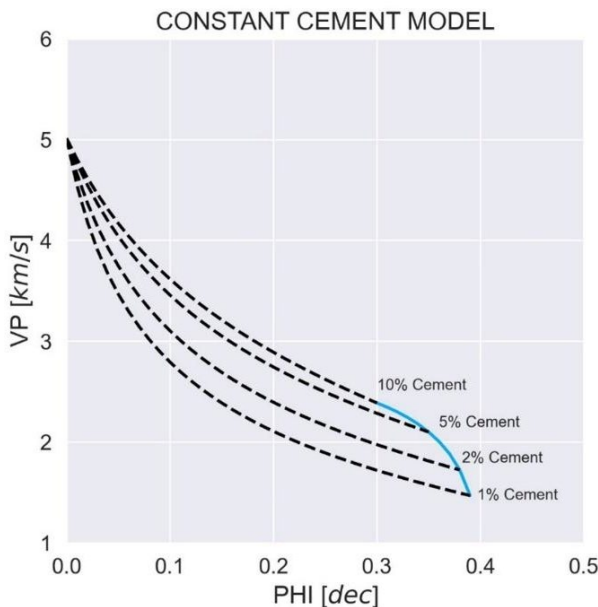

Figure 4: Example of the constant cement model for cement volumes equal to 1%, 2%, 5%, and 10%. *[dec] represents the decimal unit.*

An important parameter of these contact models is the coordination number n. In the example shown in [Figure 4](#), we used a constant n value. A possible way

to find an adequate coordination number is choosing the value that gives the best fit to the observed data. We made it searching the model that produced the smallest mean absolute percentage error, E:

$$E = \frac{1}{m}\sum_{i=0}^{m}\|\frac{(Vp_{i,model} - Vp_{i,data})}{Vp_{i,data}}\| \qquad (19)$$

where $Vp_{i,model}$ is the modeled velocity; $Vp_{i,data}$ is the velocity log; and m is the dimension of the data vector.

Velocity Curve Modeling

The last step of the proposed method is the compressional wave velocity estimation in Well B from the soft sand and constant cement models calibrated in Well A. Then, we compared the results for both cases. In this application the parameters used in rock physics modeling of velocity in the application well (Well B) are not known. The solid phase values are the same as those used for the calibration well (Well A). However, the fluid parameters are entered from the well in question (Well B). Finally, [equation 19](#) is used to estimate the error between the original and the modeled curve. Also, the correlation coefficient between these two curves is calculated. The purpose of this step is to show that, even with a limited amount of information, it is possible to use rock physics models to obtain reliable values.

RESULTS AND DISCUSSION
Well Log Evaluation

The acquired and estimated logs of Well A are illustrated in [Figure 5](#). The investigation interval presents high gamma ray (GR), as expected for feldspar-rich sandstones, and the neutron (NPHI) and bulk density (RHOB) curve crossover indicating a predominantly sandstone interval with sparse interbedded shales. The photoelectric factor (PEF) log has low values with peaks that correspond to the shale layers. This good correlation with the lithology is important for the application of mineralogical inversion, because the model will be able to better discriminate the presence of different minerals. Clay volume remains around 20%, total and effective porosities present average values of 28% and 23%, respectively, and water saturation around 20%. These calculated reservoir properties show that this well has a high exploratory potential.
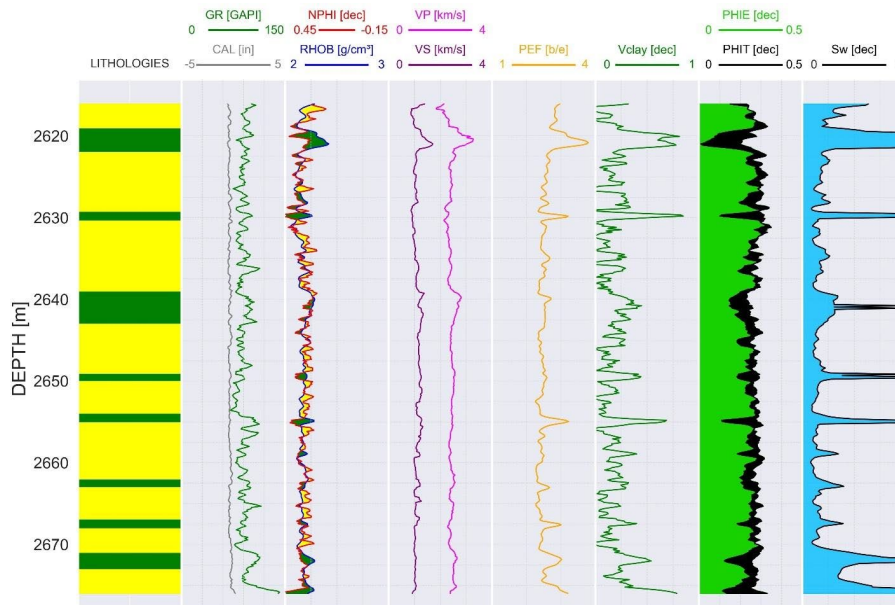
Figure 5: Registered and calculated well logs in Well A. Tracks: 1) sandstones (yellow) and shale (green); 2) caliper (gray) and gamma ray (green); 3) bulk density (blue) and neutron (red); 4) compressional wave velocity (magenta) and shear wave velocity (purple); 5) photoelectric factor (orange); 6) clay volume (green); 7) total porosity (black) and effective (light green); 8) water saturation (light blue). The GR log values are high in sandstone and shale. The NPHI-RHOB curve crossover presents interbedded shales with a good correlation with lithology profile. PEF log peaks occur in shaly intervals. These high clay volume estimates lead to low effective porosity and 100% water saturation.
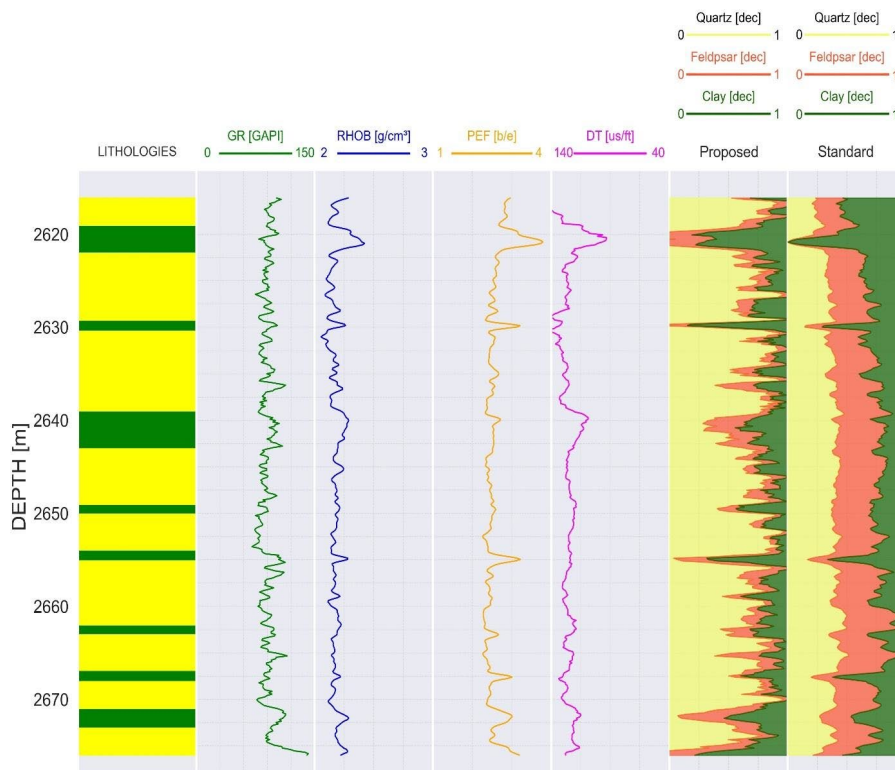
Figure 6: Well logs used in the mineralogical inversion in Well A and estimated mineral volumes. Tracks: 1) sandstones (yellow) and shale (green); 2) gamma ray (green); 3) bulk density (blue); 4) photoelectric factor (orange); 5) compressional wave slowness (magenta); 6) volumes of quartz (yellow), feldspar (red) and clay (green) estimated from our proposed methodology; 7) volumes of quartz (yellow), feldspar (red) and clay (green) from the standard methodology. Clay minerals are present over the interest interval, with peaks correlating to high RHOB and PEF logs. The predominance of quartz is expected in sandstone reservoirs, with small amounts of feldspar. Low DT values are identified in the shale between 2619/2622 m and 2639/2643 m.

Mineral Volume Estimation

The results of mineralogical inversions obtained from the GR, RHOB, PE, and DT logs are presented in Figure 6. The result from the standard methodology overestimates the clay volume in the interest interval, despite the fact that it identifies some peaks that were estimated from the neutron and density log method. Furthermore, the volume of quartz is lower than expected for arcosean sandstones. Thus, we disregarded the result of mineralogical inversion from the standard approach. In our proposed methodology, quartz mineral is predominant in the target interval, as expected, with an average value of 64%, accompanied by 16% of feldspar. Thus, even a small amount of feldspar may have a great impact on GR log. It is important to highlight a tendency of increasing feldspar volume in higher clay volume intervals (e.g., 2619/2622 m and 2671.5/2673 m intervals). A possible cause for this behavior is that both feldspar and clay minerals have the same response in some logs, as in the photoelectric factor log. As clay minerals were not introduced in the inversion process, it may associate a large increase in photoelectric factor in shaly intervals with an increase in feldspar content.

Note that the overestimation of feldspars is not an issue for the fluid substitution since it is performed over the sandstones. The rock physics models are calibrated only on sandstones using the mean effective bulk modulus of the solid phase, with the respective mineral volumes estimated in the inversion process.

Rock Physics Model Calibration

We calibrated the soft sand and constant cement models to the sandstones in Well A for the sandstones fully water saturated. The crossplot of total porosity (PHIT) and compressional wave velocity (VP) and the fitted models are shown in Figure 7. Most of the points have porosity in the range of 22 – 35% and velocity between 2.3 – 3.0 km/s. There is a tendency of increasing velocity with decreasing porosity, except for a few outliers.

Mineral volumes and their elastic properties are crucial for model calibration. In the fitted models, the value of the coordination number n obtained was equal to 6.7, with an error of 3.12%. Both models produced similar results, except for porosity greater than 37%, where the CCM exhibits a high velocity decrease with increasing porosity.

Compressional Wave Velocity Estimation

We estimate the compressional wave velocity in Well B for the soft sand and constant cement models (Figure 8). The results are equivalent for porosity lower than 37%, so we show compressional wave velocity from CCM only in the interval with porosity greater than 37%. In this interval, the SSM prediction is closer to the original VP. The modeled velocity data agree very well with the acquired log, except for the intervals 2622/2631 m and 2662/2667 m. The mean absolute percentage error between the original and modeled curves is 2.9% and the linear correlation coefficient is 64%, indicating that the model predictions are generally very good. The crossplot for the estimated and original compressional wave velocities in Well B is illustrated in Figure 9. The agreement is satisfactory, near the straight line that represents the ideal fit. The estimated VP values tend to lie below the straight line for high clay volumes.

CONCLUSION

We present a workflow for modeling the compressional wave velocity curve based on well log evaluation, mineralogical inversion and rock physics model calibration. There is a very good agreement between modeled and original logs for reservoir interval, with a mean absolute percentage error of approximately 2.9%. The clay volume estimation was consistent with the sections of shale beds described in the lithological log, showing that the use of neutron and bulk density log is the suitable one for determining the clay volume in arcosean sandstones in these two wells. The mineralogical inversion approach proved to be adequate to infer the mineral proportions within the expected range for arcosean sandstones. This result contributed to the next steps of fluid substitution and rock physics model calibration with known mineral properties. The soft sand model had the best performance in velocity modeling for porosity values above 37%, with a low or zero influence of cement in these reservoirs.
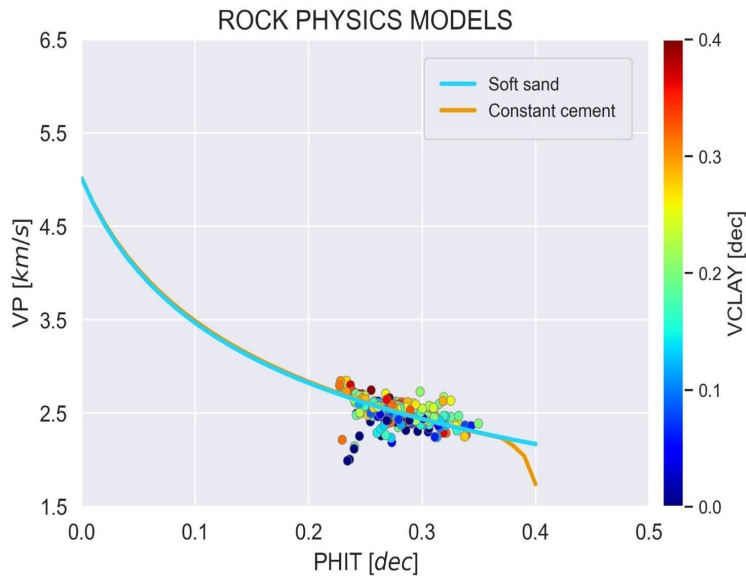
Figure 7: Crossplot of total porosity (PHIT) and compressional wave velocity (VP) showing the calibrated soft sand (blue) and constant cement (orange) rock physics models. Both models fit the data well at the whole range of velocities, except in some outliers. Clay volume estimation shows that VP increases with VCLAY at the same porosity values. *[dec] represents the decimal unit.*
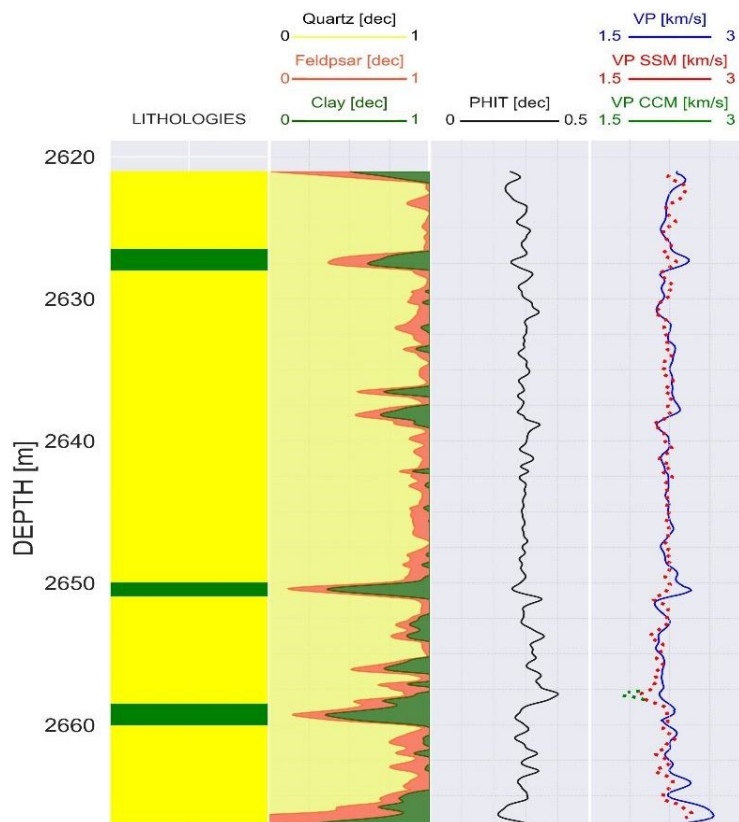

Figure 8: Result of compressional wave velocity modeling for Well B. Tracks: 1) sandstone (yellow) and shale (green); 2) volumes of quartz (yellow), feldspar (red) and clay (green); 3) total porosity (black); 4) original compressional wave velocity log (blue), compressional wave velocity log modeled with soft sand (red dots) and compressional wave velocity log modeled with constant cement (green dots). The clay volume in Well B is lower compared to Well A, and there are only three shale bodies identified in the lithological profile. The average volumes of quartz, feldspar, and clay in Well B are 81%, 11%, and 8%, respectively. The total porosity is high in the interest interval, with an average of 30%. The results of VP modeling using calibrated rock physics models show good visual correlation with the original VP log.
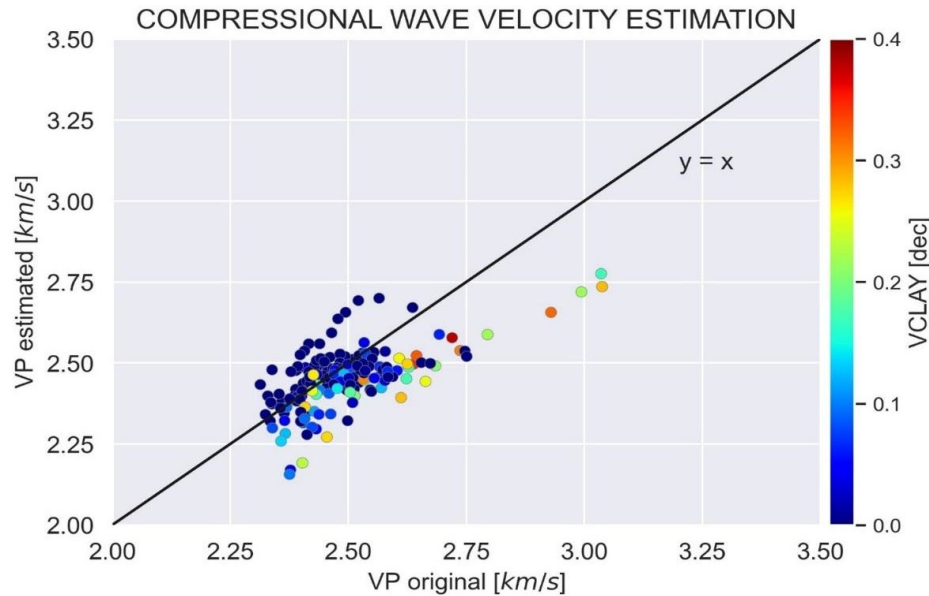
Figure 9: Crossplot between original and estimated compressional wave velocity logs colored according to the clay volume log for Well B. The black line corresponds to y=x, or exact model prediction. Points with low clay volume (blue tones) tend to be above the line, with slightly overestimated velocities, while points with high clay volume (red and yellow tones) present underestimated velocities and lie below the line. *[dec] represents the decimal unit.*

REFERENCES

Allo, F., 2019, Consolidating rock-physics classics: A practical take on granular effective medium models: The Leading Edge, **38**, 5, 334–340. DOI: 10.1190/tle38050334.1.

Amosu, A., and Y. Sun, 2018, MinInversion: a program for petrophysical composition analysis of geophysical well log data: Geosciences, **8**, 2, 65. DOI: 10.3390/geosciences8020065.

Archie, G.E., 1942, The electrical resistivity log as an aid in determining some reservoir characteristics: Transactions of the AIME, **146**, 01, 54–62. DOI: 10.2118/942054-G.

Aster, R.C., C.H. Thurber, and B. Borchers, 2013, Parameter estimation and inverse problems, 2nd ed.: Academic Press, 376 pp. DOI: 10.1016/C2009-0-61134-X.

Avseth P., T. Mukerji, and G. Mavko, 2005, Quantitative Seismic Interpretation. Applying Rock Physics Tools to Reduce Interpretation Risk: Cambridge, Cambridge University Press, 408 pp. DOI: 10.1017/CBO9780511600074.

Batzle, M., and Z. Wang, 1992, Seismic properties of pore fluids: Geophysics, **57**, 11, 1396–1408. DOI: 10.1190/1.1443207.

Bhuyan, K., and Q.R. Passey, 1994, Clay estimation from GR and neutron-density porosity logs: SPWLA 35th Annual Logging Symposium, Society of Petrophysicists and Well-Log Analysts, Tulsa, Oklahoma, paper SPWLA-1994-DDD.

Castagna, J.P., M.L. Batzle, and R.L. Eastwood, 1985, Relationships between compressional-wave and shear-wave velocities in clastic silicate rocks: Geophysics, **50**, 4, 571–581. DOI: 10.1190/1.1441933.

Doveton, J.H., 1994, Geologic log analysis using computer methods: American Association of Petroleum Geologists, AAPG Computer Applications in Geology, n. 2, Oklahoma, U.S.A., 169 pp. DOI: 10.1306/CA2580.

Dvorkin, J., and A. Nur, 1996, Elasticity of high-porosity sandstones: Theory for two North Sea data sets: Geophysics, **61**, 5, 1363–1370. DOI: 10.1190/1.1444059.

Dvorkin, J., M.A. Gutierrez, and D. Grana, 2014, Seismic reflections of rock properties. Cambridge: Cambridge University Press, 388 pp. DOI: 10.1017/CBO9780511843655.

Ellis, D.V., and J.M. Singer, 2007, Well logging for earth scientists: vol. 692, Dordrecht, Springer. 708 pp. DOI: 10.1007/978-1-4020-4602-5.

Fernandes, F.J.D., I.L. de Jesus, and W.M. Lupinacci, 2021, Influence of clay volume estimation on net-pay in well 6-BRSA-497-ESS, New Jubarte Field, Campos Basin: 17th International Congress of the Brazilian Geophysical Society & EXPOGEF. SBGf. Rio de Janeiro, Brazil.

Freire, A.F.M., G.F.R. dos Santos, C.F. da Silva, and W.M. Lupinacci, 2020, Recognition of turbidite stages in the Massapê oil field, Recôncavo Basin-Brazil, using well logs: Journal of Petroleum Science and Engineering, **192**, 107279. DOI: 10.1016/j.petrol.2020.107279.

Gassmann, F., 1951, Über die Elastizität poröser Medien: Vierteljahrsschrift der Naturforschenden Gesellschaft in Zürich, **96**, 1–23.

Greenberg, M.L., and J.P. Castagna, 1992, Shear-wave velocity estimation in porous rocks: theoretical formulation, preliminary verification and applications: Geophysical Prospecting, **40**, 2, 195–209. DOI: 10.1111/j.1365-2478.1992.tb00371.x.

Guimarães, M.D.S.B., P.S. Denicol, and R.M.R. Gomes, 2008, Avaliação e caracterização de reservatórios laminados: comparação entre as ferramentas convencionais e o perfil de indução multicomponente: Revista Brasileira de Geociências, **38**, Suppl. 1, 188–206. DOI: 10.25249/0375-7536.2008381S188206.

Han, D.H., A. Nur, and D. Morgan, 1986, Effects of porosity and clay content on wave velocities in sandstones: Geophysics, **51**, 11, 2093–2107. DOI: 10.1190/1.1442062.

Hartmann, D.J., and E.A. Beaumont, 1999, Predicting Reservoir System Quality and Performance, *in* Beaumont, E.A., and N.H. Foster, eds., Exploring for Oil and Gas Traps: Treatise of Petroleum Geology, Handbook of Petroleum Geology. Critical Elements of the Trap: Chapter 9. DOI: 10.1306/TrHbk624C9.

Harvey, P.K., J.F. Bristow, and M.A. Lovell, 1990, Mineral transforms and downhole geochemical measurements: Scientific Drilling, **1**, 4, 163–176.

Hashin, Z., and S. Shtrikman, 1963, A variational approach to the theory of the elastic behaviour of multiphase materials: Journal of the Mechanics and Physics of Solids, **11**, 2, 127–140. DOI: 10.1016/0022-5096(63)90060-7.

Hertz, H., 1882, Über die Berührung fester elastischer Körper: Journal für die reine und angewandte Mathematik, **92**, 156–171. DOI: 10.1515/9783112342404-004.

Mavko, G., C. Chan, and T. Mukerji, 1995, Fluid substitution: Estimating changes in V_P without knowing V_S: Geophysics, **60**, 6, 1750–1755. DOI: 10.1190/1.1443908.

Mavko, G., T. Mukerji, and J. Dvorkin, 2009, The Rock Physics Handbook: Tools for Seismic Analysis of Porous Media: Cambridge University Press, 511 pp. DOI: 10.1017/CBO9780511626753.

Mindlin, R.D., 1949, Compliance of elastic bodies in contact: J. Appl. Mech., ASME, **16**, 259–268. DOI: 10.1115/1.4009973.

Paiva, M.F.B., W.M. Lupinacci, A.F.M. Freire, and J. Hansford, 2019, Comparison of methodologies to estimate the clay content – A case study in the Roncador Field, Campos Basin: 16th International Congress of the Brazilian Geophysical Society & EXPOGEF. SBGf, Rio de Janeiro, Brazil. DOI: 10.22564/16cisbgf2019.091.

Pickett, G.R., 1963, Acoustic character logs and their applications in formation evaluation. Journal of Petroleum Technology, **15**, 06, 659–667. DOI: 10.2118/452-PA.

Raymer, L.L., E.R. Hunt, and J.S. Gardner, 1980, An improved sonic transit time-to-porosity transform: SPWLA 21st Annual Logging Symposium, Society of Petrophysicists and Well-Log Analysts, Lafayette, Louisiana, paper SPWLA-1980-P.

Rider, M.H., and M.C. Kennedy, 2002, The Geological Interpretation of Well Logs, 2nd ed.: Rider-French Consulting Ltd., Whittle Publishing, Rogart, 280 pp.

Savre, W.C., 1963, Determination of a more accurate porosity and mineral composition in complex lithologies with the use of the sonic, neutron and density surveys: Journal of Petroleum Technology, **15**, 09, 945–959. DOI: 10.2118/617-PA.

Schmoker, J.W., and C.J. Schenk, 1988, Facies composition calculated from the sonic, neutron, and density logs suite, upper part of the Minnelusa Formation, Powder River Basin, Wyoming: Mountain Geologist, United States, **25**, 3, 103–112.

Schön, J.H., 2015, Physical properties of rocks: Fundamentals and principles of petrophysics, 2nd ed.: Elsevier, 512 pp.

Silva, A.J.C.L.P., M.A.N.F. Aragão, and A.J.C. Magalhães, 2008, Ambientes de Sedimentação Siliciclástica do Brasil: São Paulo, Brazil, Editora Beca, 343 pp.

Tixier, M.P., and R.P. Alger, 1967, Log evaluation of non-metallic mineral deposits: SPWLA 8th Annual Logging Symposium, Society of Professional Well Log Analysts, Houston, Texas, paper SPWLA-1967-R.

Williams, D.M., 1990, The acoustic log hydrocarbon indicator: SPWLA 31st Annual Logging Symposium, Society of Petrophysicists and Well-Log Analysts, Lafayette, Louisiana, paper SPWLA-1990-W.

Winter, W.R., R.J. Jahnert, and A.B. França, 2007, Bacia de Campos: Boletim de Geociências da Petrobras, **15**, 2, 511–529.